Neutronic analysis of the European Sodium Fast Reactor: Part II - burnup results

Fridman, E.; Álvarez-Velarde, F.; Romojaro-Otero, P.; Tsige-Tamirat, H.; Jiménez-Carrascosa, A.; García-Herranz, N.; Bernard, F.; Gregg, R.; Krepel, J.; Massara, S.; Poumerouly, S.; Girardi, E.; Mikityuk, K.;

Originally published:

October 2021

Journal of Nuclear Engineering and Radiation Science 8(2022)1, 011302

DOI: https://doi.org/10.1115/1.4048765

Perma-Link to Publication Repository of HZDR:

https://www.hzdr.de/publications/Publ-31098

Neutronic analysis of the European Sodium Fast Reactor:

Part II - burnup analysis

Emil FRIDMAN
Helmholtz-Zentrum Dresden-Rossendorf (HZDR)
Bautzner Landstraße 400, 01328 Dresden, Germany
e.fridman@hzdr.de

Francisco ÁLVAREZ VELARDE
CIEMAT
Av. Complutense, 40, 28040 Madrid, Spain
francisco.alvarez@ciemat.es

Pablo ROMOJARO OTERO
CIEMAT (currently at SCK·CEN)
Av. Complutense, 40, 28040 Madrid, Spain
Pablo.Romojaro@ciemat.es **(Pablo.romojaro@sckcen.be)**

Haile TSIGE-TAMIRAT
European Commission / Joint Research Centre Petten
Westerduinweg 3. 1755LE Petten
Haileyesus.TSIGE-TAMIRAT@ec.europa.eu

Antonio JIMÉNEZ CARRASCOSA
Universidad Politécnica de Madrid (UPM)
José Gutiérrez Abascal, 2, 28006 Madrid, Spain
antonio.jcarrascosa@upm.es

Nuria GARCÍA HERRANZ
Universidad Politécnica de Madrid (UPM)
José Gutiérrez Abascal, 2, 28006 Madrid, Spain
nuria.garcia.herranz@upm.es

Franck BERNARD
Institute for Radiation Protection and Nuclear Safety (IRSN)
31 Avenue de la Division Leclerc, 92260 Fontenay-aux-Roses, France
franck.bernard@irsn.fr

Robert GREGG
National Nuclear Laboratory (NNL)
Chadwick House, Warrington WA3 6AE, UK
robert.wh.gregg@nnl.co.uk

Jiri KREPEL
Paul Scherrer Institut (PSI)
5232 Villigen, Switzerland
jiri.krepel@psi.ch

Simone MASSARA
EDF-R&D, EDF Lab Paris-Saclay
7 Boulevard Gaspard Monge, 91120 Palaiseau, France
simone.massara@edf.fr

Sandra POUMEROULY
EDF-R&D, EDF Lab Paris-Saclay
7 Boulevard Gaspard Monge, 91120 Palaiseau, France
sandra.poumerouly@edf.fr

Enrico GIRARDI
EDF-R&D, EDF Lab Paris-Saclay
7 Boulevard Gaspard Monge, 91120 Palaiseau, France
enrico.girardi@edf.fr

Konstantin MIKITYUK
Paul Scherrer Institut (PSI)
5232 Villigen, Switzerland
konstantin.mikityuk@psi.ch

Abstract

In the framework of the Horizon 2020 project ESFR-SMART, the European Sodium Fast Reactor (ESFR) core was updated through a safety-related modification and optimization of the core design from the earlier FP7 CP-ESFR project.

This study is dedicated to neutronic analysis of the new SFR core. The conducted work is reported in two parts. Part I dealt with the evaluation of the safety-related neutronic parameters of the fresh core carried out by 8 organizations using both continuous energy Monte Carlo and deterministic computer codes. A special emphasis was put on the calibration and verification of the computational tools involved in the analyses.

Part II is devoted to once-through and realistic batch-wise burnup calculations aiming at the establishing of the equilibrium core state, which will later serve as a basis for detailed safety analyses.

1. Introduction

The ESFR-SMART (European Sodium Fast Reactor Safety Measures Assessment and Research Tools) is a four-year collaborative project co-funded by European Commission within the Euratom research and training programme [1]. The project has been launched to enhance further the safety of the commercial-size European Sodium Fast Reactor (ESFR) investigated within the earlier CP-ESFR project [2].

At the initial stage of the project, the modified ESFR core design was obtained through the two-step optimization procedure applied to the ESFR-CONF2 core from CP-ESFR. The new ESFR core design was established by optimizing neutronic, thermal-hydraulic, and fuel performance using multi-physics and multi-objective optimization as reported in [3], [4]. The core design modifications were aimed at improving the core map symmetry, optimizing the void effect, and facilitating the corium relocation toward the corium catcher.

The main objective of the current study is a neutronic characterization of the new ESFR core. The conducted work is reported in two parts. Part I focused on the evaluation of the safety-related neutronic parameters of the fresh core, which are used to calibrate and verify the computer codes used in the analyses [5]. Part II of the paper is devoted to once-through and realistic batch-wise burnup analysis aiming at the establishing of the equilibrium core loading configuration, which will later serve as a basis for detailed safety analyses.

Part II of the paper is structured as follows. Section 2 provides a brief overview of the initial ESFR core. Section 3 discusses the modeling assumptions. Results are presented in Section 4. Section 5 summarizes the paper. Facilitation

2. A brief description of the initial ESFR-SMART core

This section provides a brief description of the new ESFR core and summarizes the major core parameters. The core description is similar to that given in Part I of the paper [5] and provided here to facilitate the reading.

The radial core layout is shown in Figure 1. The core consists of inner fuel (IF) and outer fuel (OF) regions loaded with 216 and 288 fuel sub-assemblies (SA) respectively. In the initial core, the Pu content in both zones is equal to 17.99 wt%. Both regions are managed using a 6-batch fuel loading pattern. The core is controlled by 24 control and shutdown devices (CSD) and 12 dedicated shutdown devices (DSD). Compared to the ESFR-WH core, new corium discharge tubes (CDT) were introduced into several locations (31 in total) including the central position, the boundary between IF and OF regions, and the core periphery. The active core is surrounded by 3 rings of reflector SA, 2 rings of internal spent fuel storage positions, and 4 rings of shielding SA. A preliminary analysis, performed at CIEMAT, showed a negligible effect of the spent fuel storage and shielding on neutronics. Therefore, these regions were not considered in the neutronic analyses of the ESFR-SMART core

The axial layout of the IF and OF SAs is presented in Figure 2. Compared to the ESFR-WH core, a large sodium plenum followed by a neutron absorber was introduced above the active core. In addition, the heights of the fissile regions were reduced and fertile and steel blankets were introduced below. A single fissile enrichment was adopted for both IF and OF regions. In order to improve the radial power uniformity, the height of the IF fissile region was further reduced. At room temperature, the active core height is 1 m. The height of the blanket in IF and OF zones is 5 and 25 cm respectively. The height of the sodium plenum is 60 cm

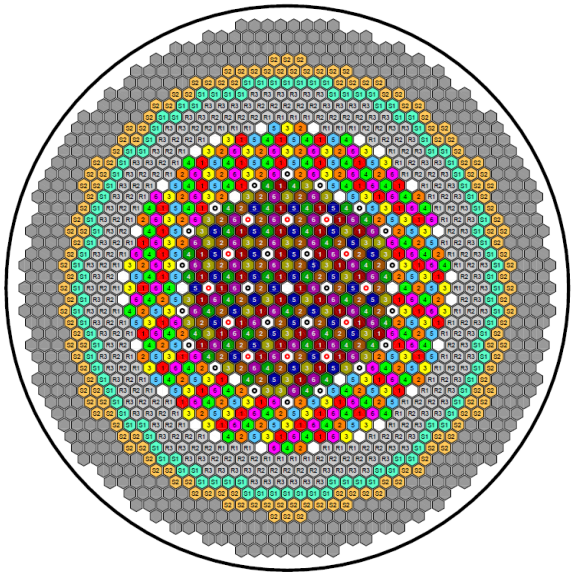

1 2 3 4 5 6	IF SA	6 batches × 36
1 2 3 4 5 6	OF SA	6 batches × 48
○ ○	CSD / DSD	24 / 12
R1 R2 R3	Reflector	66 / 96 / 102
S1	Spent IF storage	3 batches × 36
S2	Spent OF storage	3 batches × 48
⬡	CDT	31

Fig. 1 Radial core layout

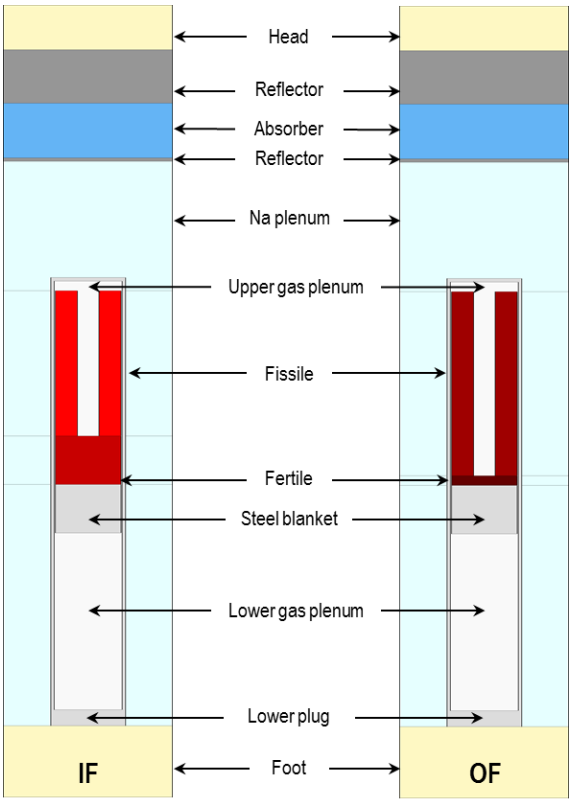

Fig. 2 Axial core layout

3. Once-through burnup calculations

3.1 Modeling assumptions

The initial core neutronic calculations reported in [5] were followed by the once-through burnup analysis. The calculations were performed for a total of 2100 effective fuel power days (EFPD) assuming all-fresh fuel with identical Pu content in all 6 fuel batches at beginning of life (BOL). Fuel SAs reloading and reshuffling was not considered. During the entire campaign, all control devices were withdrawn to a parking position that is the top of the upper gas plenum. The core power was 3600 MWth.

Concerning axial discretization the inner core was subdivided into 8 burnable regions (3 fertile + 5 fissile) while the outer core was subdivided into 6 burnable regions (1 fertile + 5 fissile). In radial directions, two options were considered:

- Option 1: Batch-wise discretization with 6 radial burnable regions in IF and OF. This option assumes that all fuel SAs, belonging to a certain batch, form a single burnable region.
- Option 2: SA-wise burnup with 216 radial burnable regions in IF and radial 288 burnable regions in OF.

Option 1 and Option 2 lead to a total of 84 and 3456 burnable regions respectively. The latter can be restrictively expensive for MC-based burnup codes. Therefore, the former was adopted as a reference discretization option. The evaluated parameters include burnup dependent quantities such as core reactivity and isotopic composition as well as axial power profiles.

The once-through burnup calculations were carried out by 7 organizations presented in Table 1. Four institutions, namely HZDR, CIEMAT, IRSN, and UPM, utilized MC-based burnup codes. The MC Serpent, applied by HZDR, includes a built-in decay and depletion solver [6]. UPM performed calculations with KENO which is coupled with ORIGEN-S depletion solver within the SCALE code system [7]. CIEMAT and IRSN used the EVOLCODE 2.0 [8] and VESTA 2.2.0 [9] codes which couple MCNP with the depletion solvers ACAB [10] and PHOENIX respectively. The deterministic results were produced by NNL employing WIMS, as well as by PSI and EDF both using ERANOS/VARIANT.

Table 1. Participants and codes used for once-through burnup calculations.

Organization	Code	Nuclear data library
HZDR	Serpent 2.1.29	JEFF-3.1
CIEMAT	EVOLCODE 2.0 (MCNP6.1.1b + ACAB) [8], [10]	JEFF-3.1
IRSN	VESTA 2.2.0 (MCNP6.1.1b + PHOENIX 2.2.0) [9]	JEFF-3.1
UPM	SCALE6.2.3 (KENO-VI + ORIGEN 6.2)	JEFF-3.1
NNL	WIMS11	JEFF 3.1.2
PSI	ERANOS/VARIANT	JEFF-3.1
EDF	ERANOS/VARIANT	JEFF-3.1

3.2 Results: once-through burnup calculations

3.2.1 Core reactivity

The burnup dependent core reactivity is plotted in Figure 3 and the differences relative to the Serpent reference are presented in Figure 4. The Serpent, EVOLCODE, and VESTA results show a good agreement over entire burnup campaign with a maximum discrepancy of 250 pcm. KENO agrees very well with Serpent at BOL. However, the differences are monotonically increasing with burnup and reaching 785 pcm at EOL, which can be attributed to the disabling of the probability tables in the unresolved resonance region. The deviation between Serpent and WIMS does not exceed 170 pcm. As compared to Serpent, the ERANOS underestimates the reactivity at BOL and predicts higher values at EOL. It is worth noting that the EOL reactivity predicted with ERANOS by PSI and EDF differs by 200 pcm.

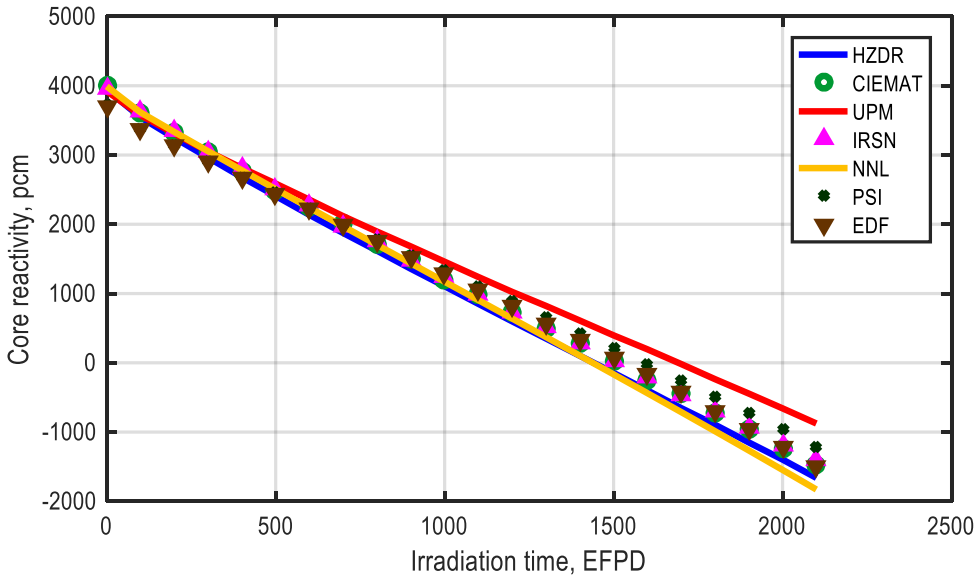

Fig. 3 Core reactivity as a function of irradiation time.

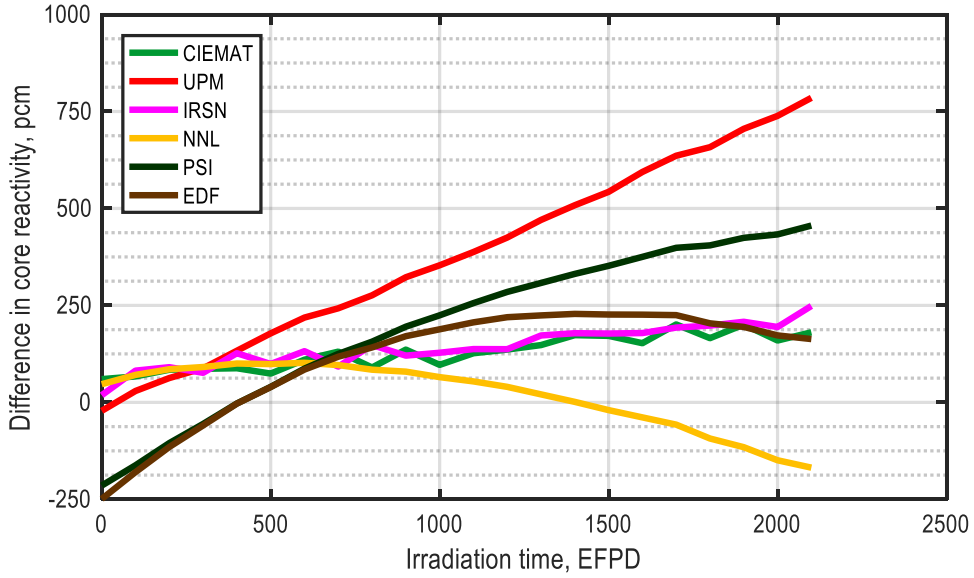

Fig. 4 Differences in core reactivity vs. Serpent.

3.2.2 Isotopic composition

The evolution of isotopic composition with burnup is presented in Figures 5-6. During the irradiation campaign, the total Pu content in the fissile regions of IF and OF stays approximately constant with a slight increase in the Pu-239 amount and a moderate reduction in Pu-241 amount (Figure 5). The amount of Am-241 increases by about 60% towards EOL.

In the fertile regions, there is a steep increase in the Pu-239 content, which constitutes about 89% of the total Pu amount at EOL (Figure 6). The share of Pu-240 reaches 10% and other Pu isotopes constitute less than 1% of the total Pu.

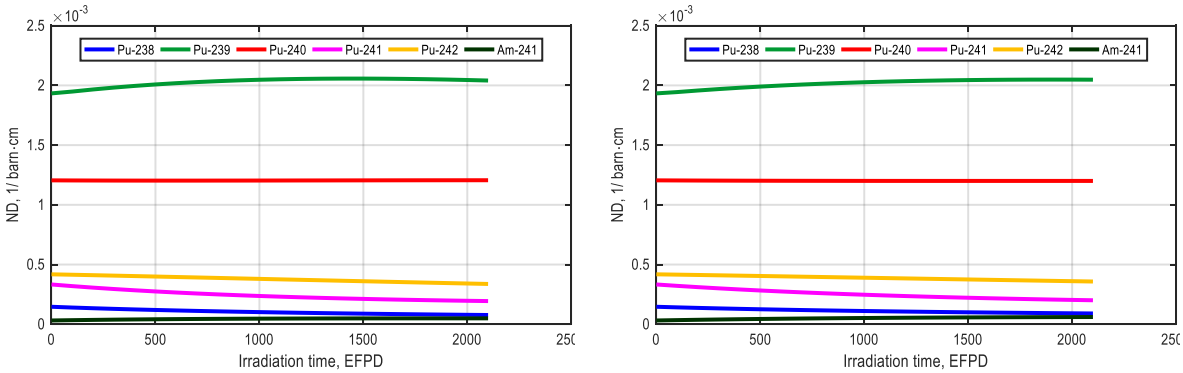

a. averaged over IF-FI b. averaged over OF-FI

Fig. 5 Evolution of isotopic composition in the fissile zones, Serpent result.

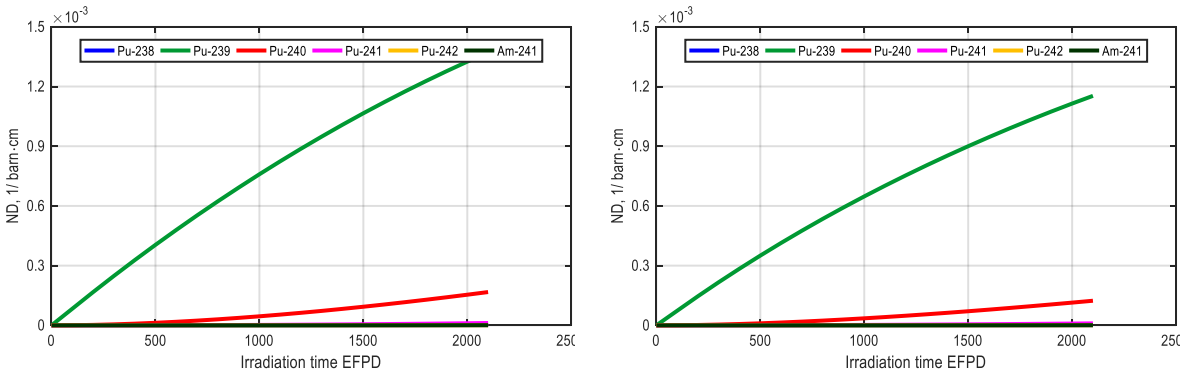

a. averaged over IF-FE b. averaged over OF-FE

Fig. 6 Evolution of isotopic composition in the fertile zones, Serpent result.

The EOL isotopic compositions of the inner and outer fissile zones predicted by the different codes show a generally good agreement (Figure 7-8). The EOL amount of Pu-239:242 and Am-241 predicted by Serpent agree within 0.4% with VESTA and KENO. The deterministic results have a slightly higher discrepancy of about 1.3% for Pu-239:242 and 2.1% for Am-241. EVOLCODE noticeably underpredicts the amount of Pu-241 and Am-241.

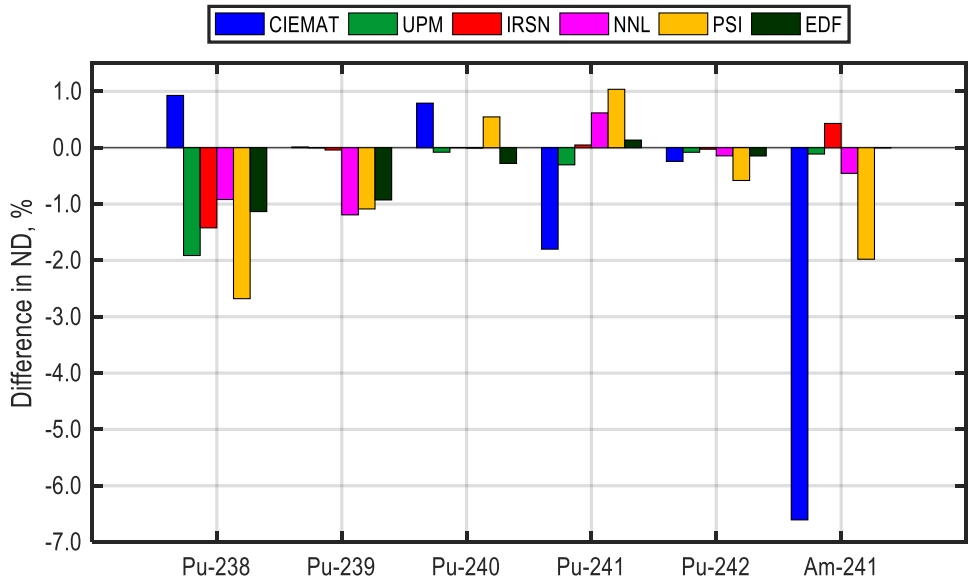

Fig. 7 Differences in isotopic composition of IF-FI at EOL vs. Serpent.

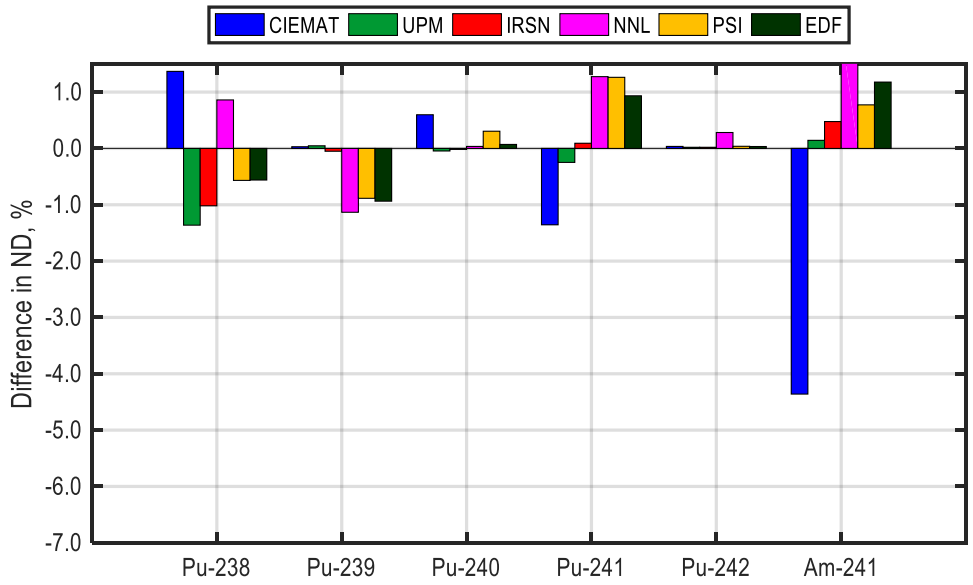

Fig. 8 Differences in isotopic composition of OF-FI at EOL vs. Serpent.

The EOL isotopic compositions of the fertile zones exhibit significantly higher spread as shown in Figures 9-10 for the inner and outer regions respectively. Compared to the reference Serpent solution, the major differences were found in the amounts of Pu-238, 241, 242 and Am-241 calculated by the deterministic codes. The corresponding results obtained with the MC-based depletion codes show much lower deviation from the reference. The amounts of the dominant Pu isotopes (i.e. Pu-239 and Pu-240), estimated by the MC codes, agree within less than 3% while the deterministic results deviate by more than 6% from those of Serpent.

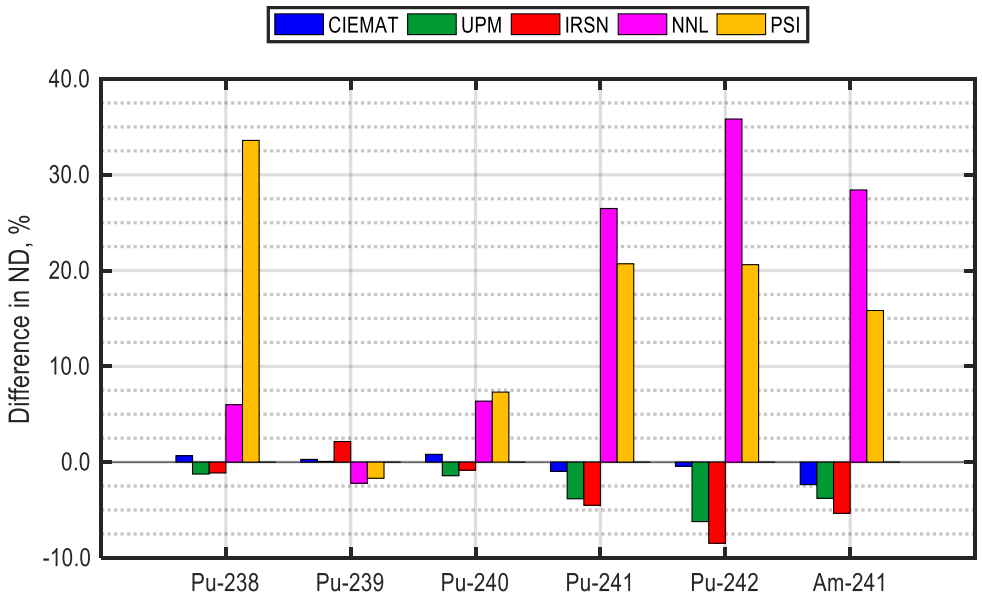

Fig. 9 Differences in isotopic composition of IF-FE at EOL vs. Serpent.

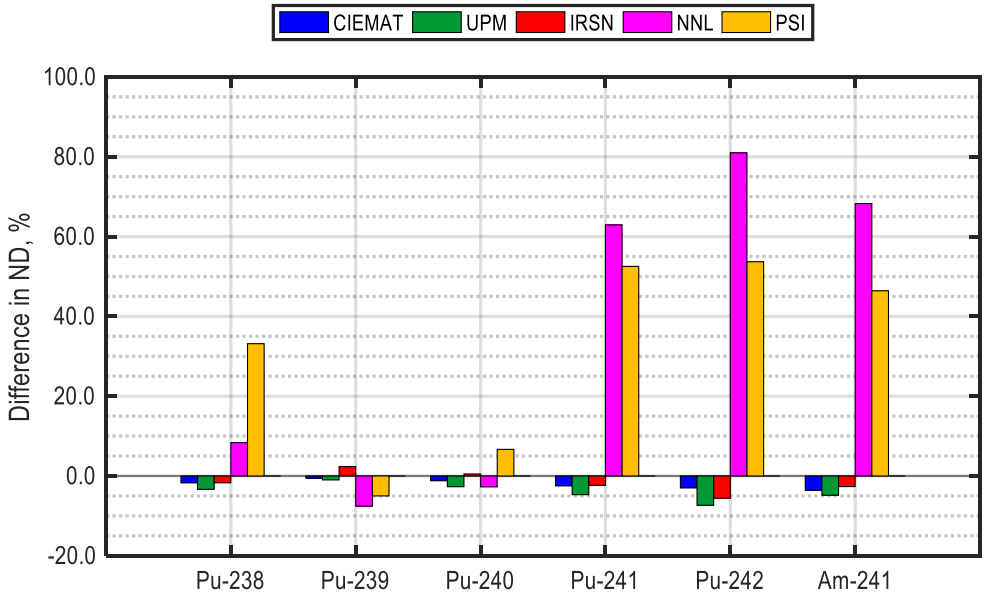

Fig. 10 Differences in isotopic composition of OF-FE at EOL vs. Serpent.

3.2.3 Axial power profiles

Region-averaged axial power profiles at BOL and EOL are depicted in Figure 11. Towards EOL, there is a clear shift in power profiles in both IF and OF regions due to Pu breeding in the lower blankets. The corresponding results provided by three organizations are in a very good agreement.

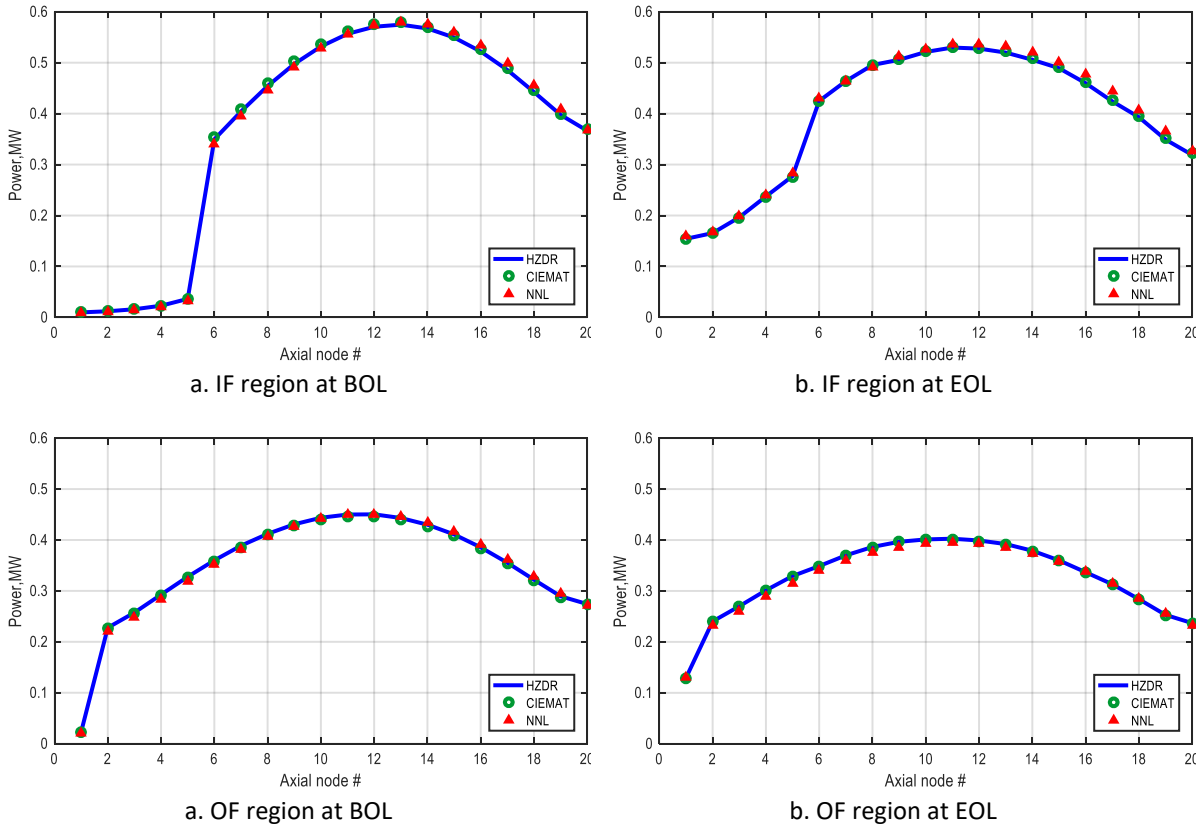

a. IF region at BOL

b. IF region at EOL

a. OF region at BOL

b. OF region at EOL

Fig. 11 Region-averaged axial power profiles.

4. Multi-batch burnup calculations

4.1 Modelling assumptions

The once-through burnup analysis, reported in Section 3, was performed in a "single-batch" mode starting with the all-fresh fuel with identical Pu content in all SAs. However, the new ESFR core was designed to be operated in a 6-batch mode. This implies that after a certain period of time, designated as a "fuel cycle", one fuel batch in both fuel regions is discharged and replaced by the fresh fuel SAs. The objective of the current study is to achieve the equilibrium 6-batch core state by performing multi-batch burnup calculations including the reloading of the fuel batches. The following modelling assumptions were made:

- The total in-core residence time of a single batch was fixed to 2172 EFPD.
- The fuel cycle length was fixed to 362 EFPD (i.e. 1/6th of the total fuel in-core residence time).
- Every fuel batch comprises 36 inner and 48 outer SAs (i.e. 1/6th of the total number of SAs).
- The fuel SAs were loaded according to the 6-batch loading scheme shown in Figure 1.
- The equilibrium core was established through the simulation of the 3 full in-core residence periods (i.e. 18 successive fuel cycles).
- The fuel SAs were managed using the re-loading scheme shown in Table 2.
- All control devises are at the parking position.
- The axial and radial core discretization was identical to "Option 1" used for the once-through burnup calculation (see Section 3.1).

Table 2. Fuel re-loading scheme for the 6-batch core showing a number of accumulated in-core residence cycles for every batch and fuel cycle. The discharged batch is shaded by green.

Batch	*Cycle 1*		*Cycle 2*		*Cycle 3*		*Cycle 4*		*Cycle 5*		*Cycle 6*	
	BOC1*	EOC1	BOC2	EOC2	BOC3	EOC3	BOC4	EOC4	BOC5	EOC5	BOC6	EOC6
1	Fresh	1	1	2	2	3	3	4	4	5	5	6
2	1	2	2	3	3	4	4	5	5	6	Fresh	1
3	2	3	3	4	4	5	5	6	Fresh	1	1	2
4	3	4	4	5	5	6	Fresh	1	1	2	2	3
5	4	5	5	6	Fresh	1	1	2	2	3	3	4
6	5	6	Fresh	1	1	2	2	3	3	4	4	5

*BOC = beginning of cycle, EOC = end of cycle

The evaluated parameters include cycle-wise core reactivity and several parameters characterizing the core at the End of Equilibrium Cycle (EOEC) state such as radial power distribution, batch-wise axial power distribution, and batch-wise axial burnup profiles. The multi-batch burnup calculations were performed by HZDR using Serpent and by PSI using ERANOS with JEFF3.1 nuclear data library.

4.2 Results: Multi-batch burnup calculations

4.2.1 Cycle-wise core reactivity

The cycle-wise core reactivity calculated by Serpent and ERANOS for 2 from 3 consecutive full in-core residence periods is presented in Figure 12 while omitting the results of the first transitional period. Although all fuel cycles were modelled sequentially, the starting point of every full in-core period in the plot was set to 0 EFPD for comparison purposes.

In Serpent case, the cycle-wise reactivity of the two presented in-core residence periods is very close and agrees within less than 20 pcm, thus, indicating the equilibrium core state. The BOC reactivity is around 1400 pcm, which is significantly lower than the BOL reactivity of about 4000 pcm in the once-through case. For both simulated periods, the BOC reactivity slightly varies from cycle to cycle. Since the fuel SAs are not shuffled within the core, this can be explained by a somewhat different reactivity worth of the different fuel batches. In all cycles, there is sufficient EOC reactivity margin of around 500 pcm.

The ERANOS results are close to those of Serpent and exhibit a similar cycle-wise behavior. However, there is somewhat higher discrepancy in reactivity between two residence periods. In the ERANOS case, the cross-sections are recalculated according to the actual burnup state only after every 6 batches, at the end of the 6 batch period. Therefore, achieving the equilibrium state may require a higher number of period calculations.

It is worth mentioning that the behavior of the reactivity curve can be quite sensitive to the nuclear data library applied. As an example, a comparison of cycle-wise reactivity obtained with two different cross sections sets (JEFF-3.1 and ENDF/B-VII.0) is shown in Figure 13.

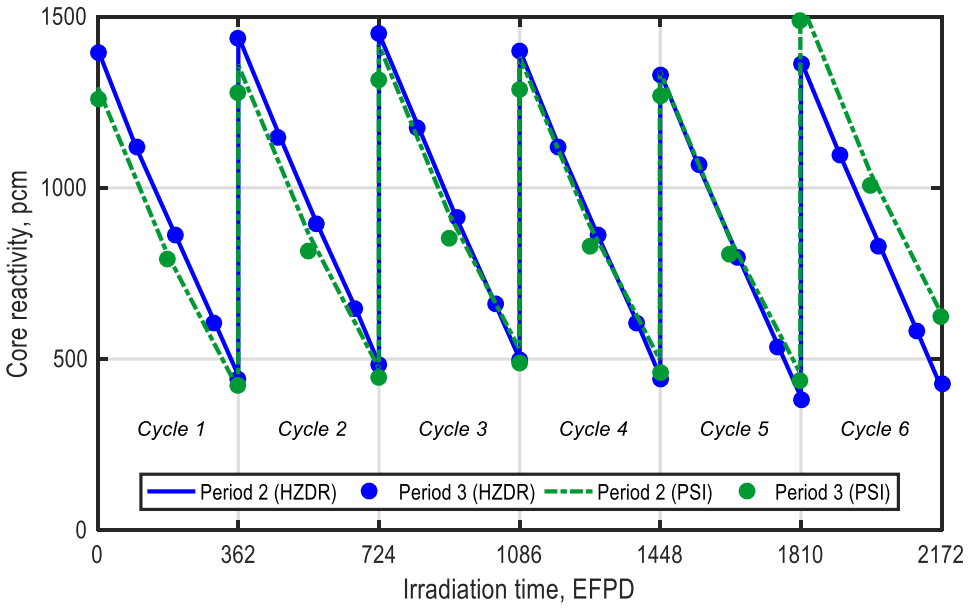

Fig. 12 Cycle-wise core reactivity for 2 consecutive full in-core residence periods.

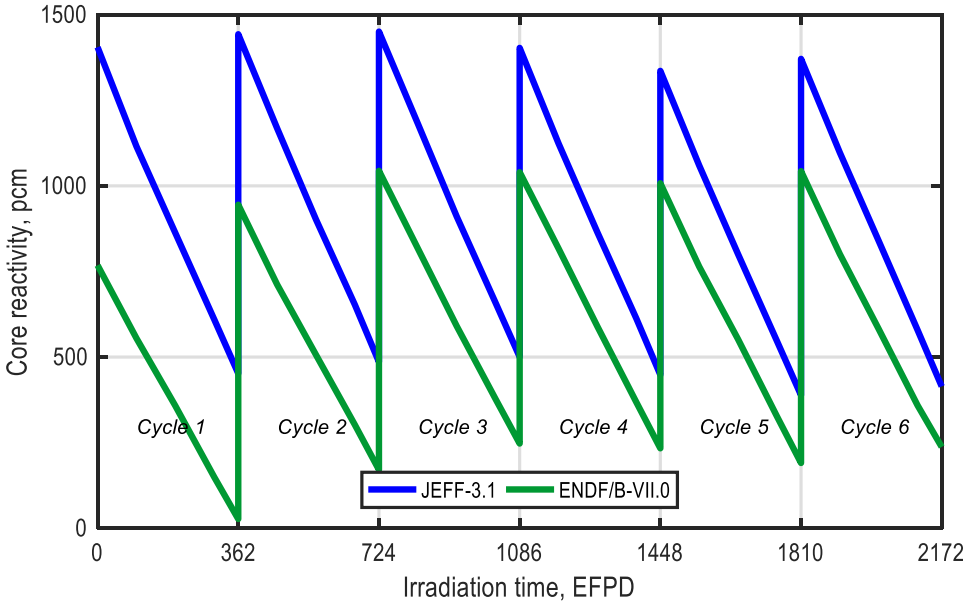

Fig. 13 Cycle-wise core reactivity obtained with two different cross sections sets.

4.2.2 Initial characterization of the EOEC core

Since the cycle-wise core behavior is approximately identical, the EOC state of the 3rd in-core residence period was considered as the EOEC state. In this section the following parameters are reported: radial power distribution (Figure 14), batch-wise axial power distribution (Figure 15 and Figure 16), and batch-wise axial burnup profiles (Figure 17 and Figure 18).

This core state will be used in the follow-up studies for further more detailed analysis. For example, the EOEC core will be studied to assess a bunch of the safety relevant parameters such as a detailed spatial distribution of Doppler constants and sodium void reactivity, decay heat distribution, and other safety-related parameters. The EOEC core will be also analyzed using coupled core thermal hydraulics and neutronics simulations. The obtained EOEC core state will also serve as a basis for the modeling of the system behavior in selected accident scenarios (both protected and unprotected).

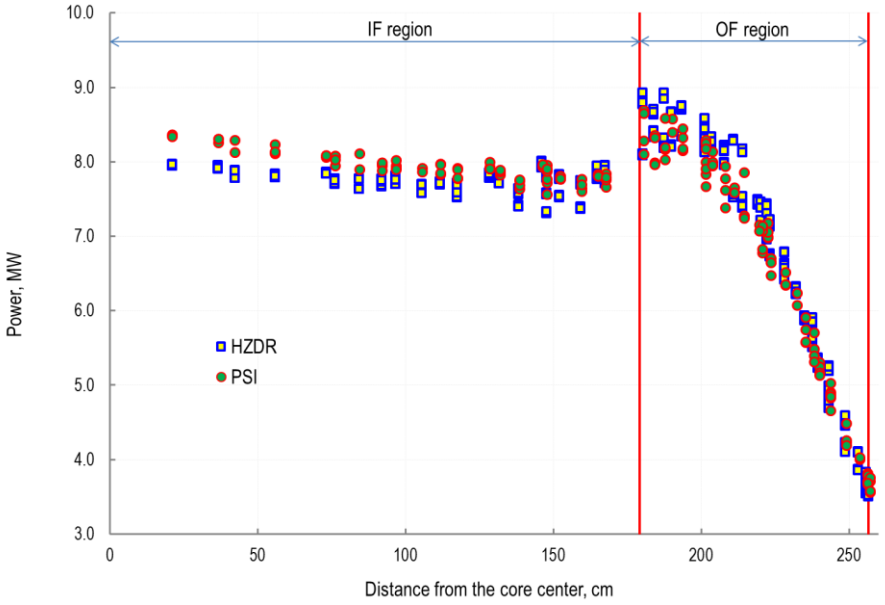

Fig. 14 Radial power profile at EOEC.

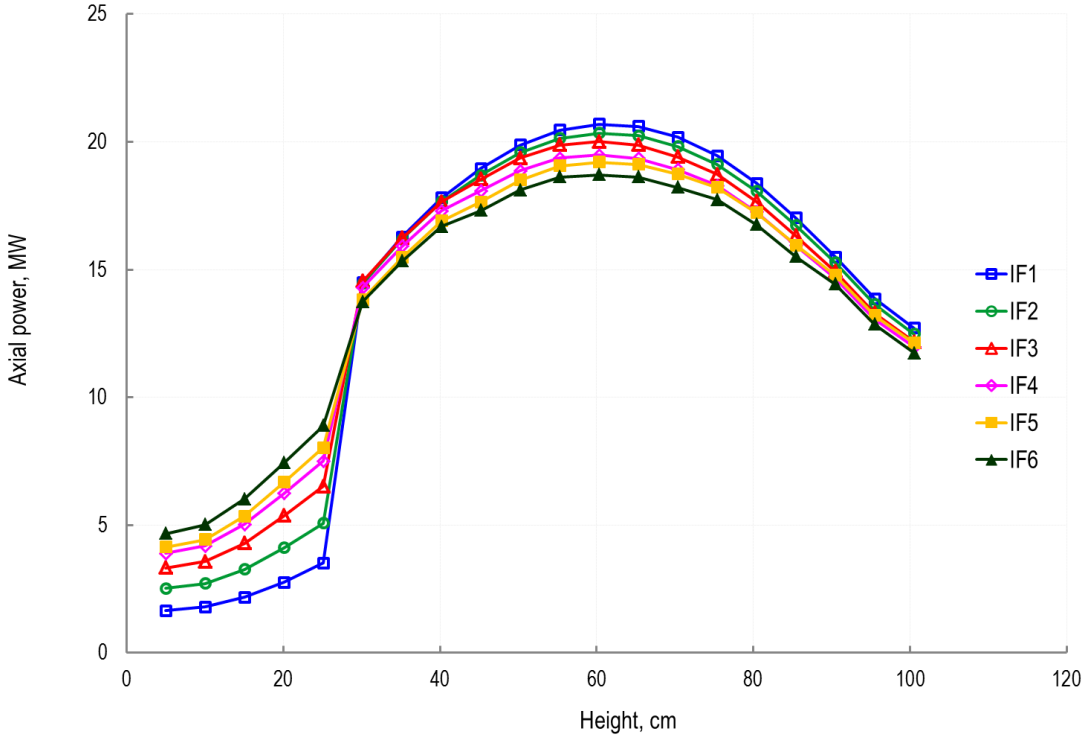

Fig. 15 IF batch-wise axial power profiles at EOEC.

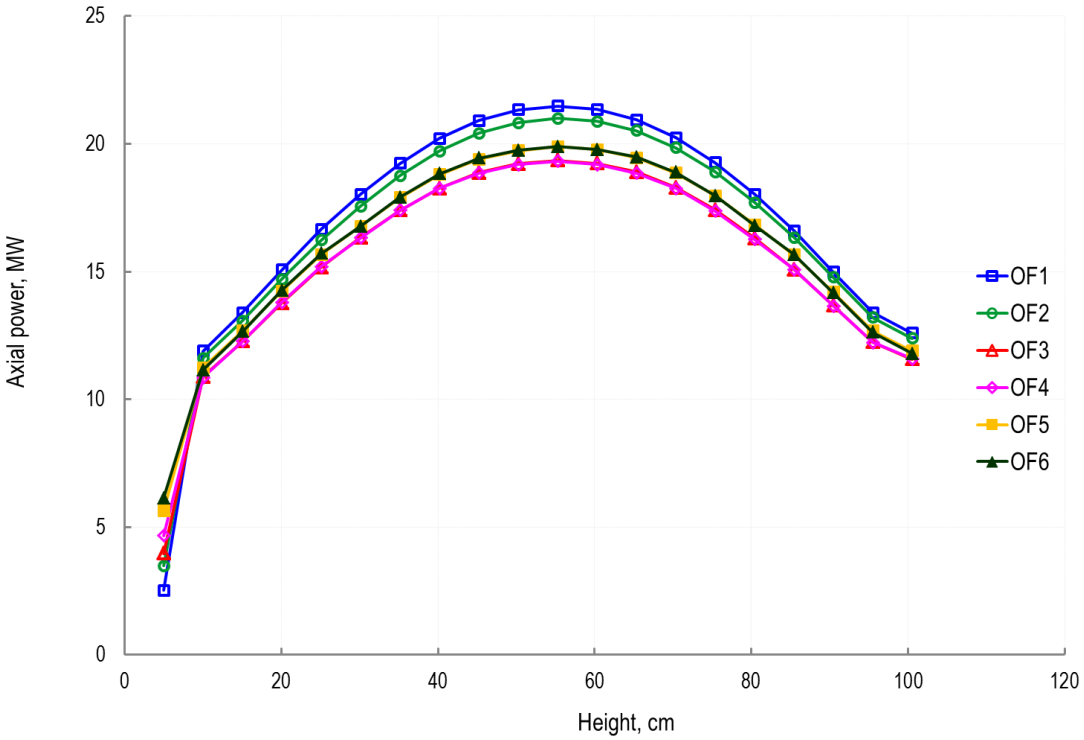

Fig. 16 OF batch-wise axial power profiles at EOEC.

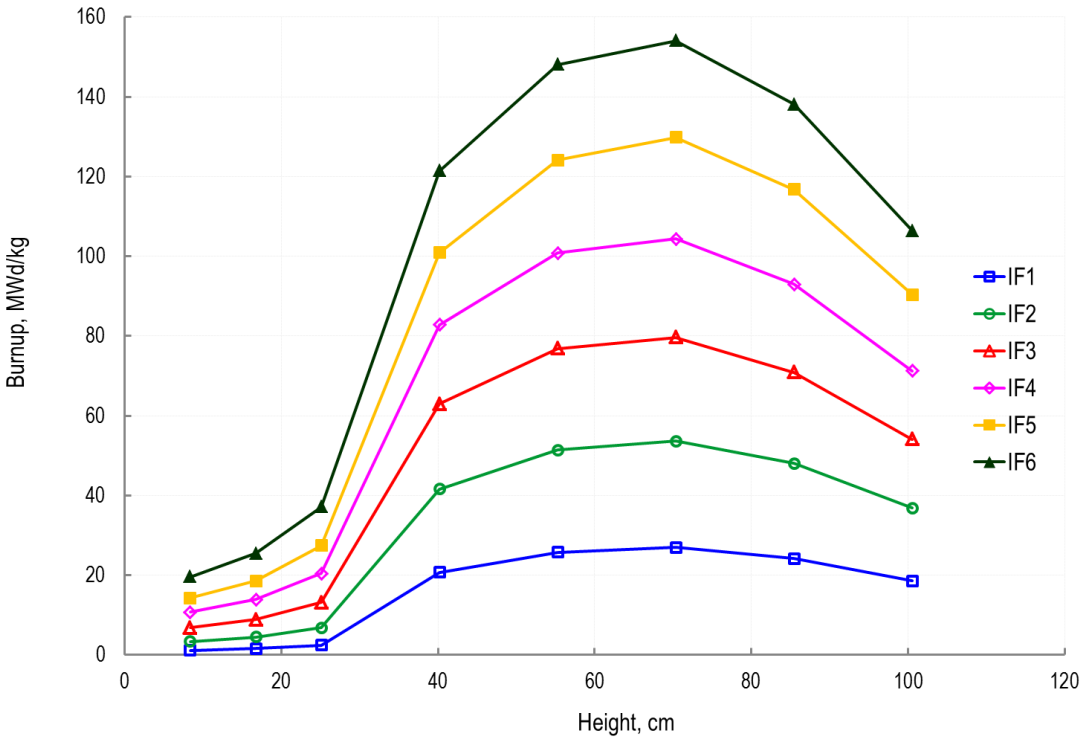

Fig. 17 IF batch-wise axial burnup profiles at EOEC.

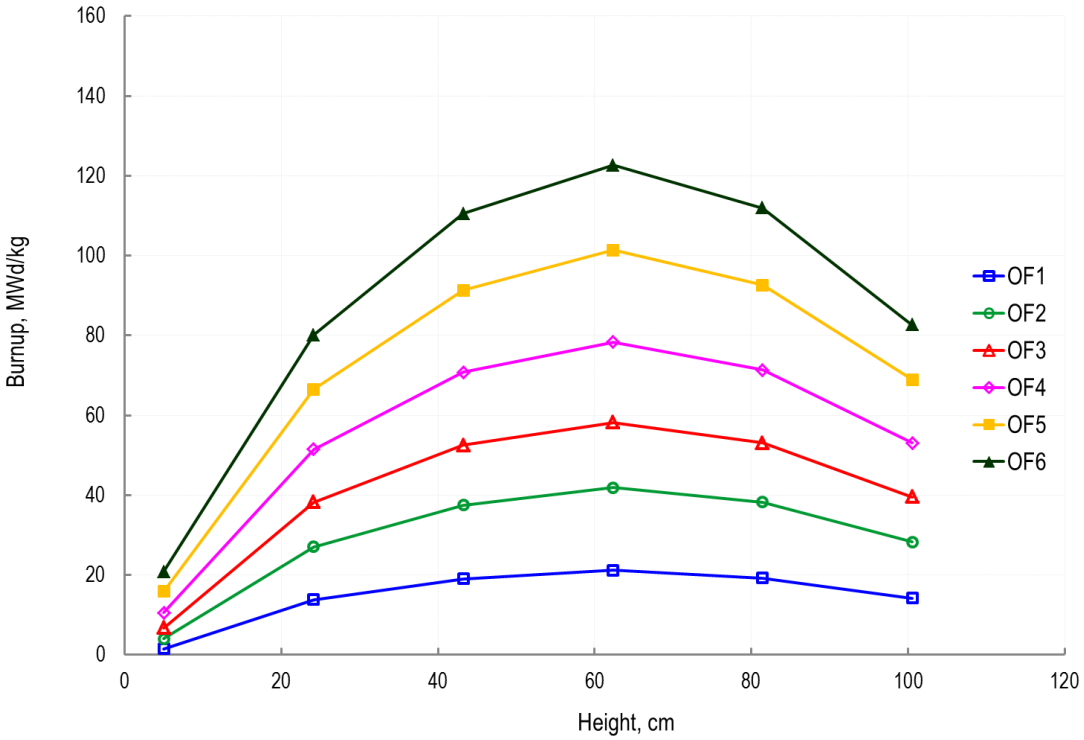

Fig. 18 OF batch-wise axial burnup profiles at EOEC.

5. Summary and conclusions

Part II of the paper reported on the burnup analysis of the newly proposed ESFR core. Initially, once-through full core burnup calculations were performed by 7 organizations using MC-based and deterministic depletion codes. The reported results, including temporal evolution of the core reactivity and isotopic compositions, show generally acceptable mutual agreement.

The once-through calculations were followed by the more realistic multi-batch burnup analysis aiming at the establishing of the equilibrium core state. The desired equilibrium 6-batch core was obtained through the simulation of the 18 successive fuel cycles, equivalent to the 3 full in-core residence periods. The EOEC core state, obtained in the current study, will be used as a basis for the follow-up more detailed analyses. This includes, for example, an assessment of the safety relevant parameters such as a detailed spatial distribution of Doppler constants and sodium void reactivity, decay heat distribution, and other safety-related parameters. The steady state performance of the EOEC core will be analyzed using coupled core thermal hydraulics and neutronics simulations. The obtained EOEC core state will be also used for the modeling of the system behavior in selected accident scenarios.

Acknowledgment

The research leading to these results has received funding from the Euratom research and training programme 2014-2018 under Grant Agreement Number 754501 (ESFR-SMART)

References

[1] K. Mikityuk *et al.*, “ESFR-SMART: new Horizon-2020 project on SFR safety,” in *IAEA FR2017*, 2017.

[2] G. L. Fiorini and A. Vasile, “European Commission – 7th Framework Programme: The Collaborative Project on European Sodium Fast Reactor (CP ESFR),” *Nucl. Eng. Des.*, vol. 241, no. 9, pp. 3461–3469, Sep. 2011.

[3] A. Rineiski, C. Meriot, M. Marchetti, and J. Krepel, “Core Safety Measures in ESFR-SMART,” in *PHYSOR 2018*, 2018.

[4] A. Rineiski *et al.*, “New core safety measures and their preliminary assessment in the ESFR-SMART project,” *J. Nucl. Eng. Radiat. Sci.*, vol. Submitted, 2020.

[5] E. Fridman *et al.*, “Neutronic analysis of the European Sodium Fast Reactor: Part I - fresh core results,” *J. Nucl. Eng. Radiat. Sci.*, vol. Submitted, 2020.

[6] M. Pusa and J. Leppänen, “Computing the Matrix Exponential in Burnup Calculations,” *Nucl. Sci. Eng.*, vol. 164, no. 2, pp. 140–150, Feb. 2010.

[7] B. T. Rearden and M. A. Jessee, “SCALE Code System,” ORNL/TM-2005/39, Oak Ridge National Laboratory, Oak Ridge, TN, Unite States, 2017.

[8] F. Álvarez-Velarde, E. M. González-Romero, and I. M. Rodríguez, “Validation of the burn-up code EVOLCODE 2.0 with PWR experimental data and with a Sensitivity/Uncertainty analysis,” *Ann. Nucl. Energy*, vol. 73, pp. 175–188, Nov. 2014.

[9] W. Haeck, B. Cochet, and L. Aguiar, “Monte Carlo depletion calculations using VESTA 2.1 new features and perspectives,” in *PHYSOR 2012*, 2012.

[10] J. Sanz, O. Cabellos, and N. García-Herranz, “ACAB-2008: Activation Code V2008,” NEA Data Bank NEA-1839, 2008.